

Article

Development and Analysis of Graphene-Sheet-Based GaAs Schottky Solar Cell for Enriched Efficiency

L. Kholee Phimu ¹, Rudra Sankar Dhar ^{1,*}, Khomdram Jolson Singh ² and Amit Banerjee ^{3,*}

¹ Department of Electronics and Communication Engineering, National Institute of Technology Mizoram, Aizawl 796012, India

² Department of Electronics and Communication Engineering, Manipur Institute of Technology, Canchipur, Imphal 795003, India

³ Microsystem Design-Integration Lab, Physics Department, Bidhan Chandra College, Asansol 713303, India

* Correspondence: rudra.ece@nitmz.ac.in (R.S.D.); amitbanerjee.nus@gmail.com (A.B.)

Abstract: Comparative studies of the 2D numerical modelling and simulation of graphene-based gallium arsenide and silicon Schottky junction solar cell are studied using TCAD tools. The performance of photovoltaic cells was examined while taking parameters, such as substrate thickness, relationship between transmittance and work function of graphene, and n-type doping concentration of substrate semiconduction. The area with the highest efficiency for photogenerated carriers was found to be located near the interface region under light illumination. The significant enhancement of power conversion efficiency was shown in the cell with a thicker carrier absorption Si substrate layer, larger graphene work function, and average doping in a silicon substrate. Thus, for improved cell structure, the maximum $J_{SC} = 4.7 \text{ mA/cm}^2$, $V_{OC} = 0.19 \text{ V}$, and fill factor = 59.73% are found under AM1.5G, exhibiting maximum efficiency of 6.5% (1 sun). The EQE of the cell is well above 60%. This work reports the influence of different substrate thickness, work function, and N-type doping on the efficiency and characteristics of graphene-based Schottky solar cells.

Keywords: external quantum efficiency; graphene; power conversion efficiency; Schottky barrier solar cell (SBSC); TCAD



Citation: Phimu, L.K.; Dhar, R.S.; Singh, K.J.; Banerjee, A. Development and Analysis of Graphene-Sheet-Based GaAs Schottky Solar Cell for Enriched Efficiency. *Micromachines* **2023**, *14*, 1226. <https://doi.org/10.3390/mi14061226>

Academic Editor: Hugo Aguas

Received: 11 March 2023

Revised: 16 May 2023

Accepted: 19 May 2023

Published: 10 June 2023



Copyright: © 2023 by the authors. Licensee MDPI, Basel, Switzerland. This article is an open access article distributed under the terms and conditions of the Creative Commons Attribution (CC BY) license (<https://creativecommons.org/licenses/by/4.0/>).

1. Introduction

Due to graphene's unique structure and characteristics, a single atomic layer has attracted significant attention, such as high mobility, low resistivity, and band gap [1]. Graphene has been created as ultrathin sheets made of a few atomic layers through mechanical exfoliation or CVD (chemical vapour deposition) and can be shifted to many substrates; thus, it will open up a large range of potential applications, including smart composites, photo sensors, and high-performance electronic devices [2]. Specifically, the graphene layer is a major material for use in the production of effective solar cells due to its exceptional combination of optical transparency and high electrical conductivity in the visible and near-infrared spectrum [3,4]. On various substrates, such as Si [5], CdS [6], CdSe [7], and GaAs [8], graphene-based Schottky junction solar cells have been produced in recent years. A Schottky junction was successfully formed on n-type GaAs by Wenjing et al., producing a power conversion efficiency of 1.95% [9]. GaAs has more radiation resistance [10] than the Si substrate, which is most frequently used, and has a direct band gap [11], which makes it suitable for highly efficient solar cells for both terrestrial and space applications. However, in order to increase solar cell efficiency, the band parameter must be studied, and various thicknesses of the structure must be optimised. We, therefore, optimised the thickness of the GaAs substrate with a graphene layer in SILVACO TCAD in this paper, and the results were confirmed using published experimental data.

The proposed graphene structure is shown in Figure 1. It consists of three regions. The ability to create graphene-on-silicon Schottky solar cells at room temperature opens up a wide

range of applications for light gathering and conversion with the benefits of environmental friendliness and lower cost [12]. In this design, the graphene sheet performs dual roles for separation of holes/electrons as an active layer and as a carrier medium for transportation, in addition to acting as a transparent electrode for the transmission of light [13]. Despite the fact that the initial energy conversion efficiency is only 1.65% [14], the performance of graphene silicon Schottky cells was improved using silicon nano-array substrate adoption [15], chemical doping [5], and a graphene/P3HT/silicon configuration [16], ranging from 1.96% up to 10.3%. Some of the critical parameters, such as surface charge recombination, work function, and graphene conductivity, played a key role in establishing the performance of the device. Still, there has not been much research conducted on Schottky barriers. Thus, considerably more consideration and study are needed for the use of graphene in Schottky solar cells. Figure 2 shows an energy band diagram of graphene solar cells.

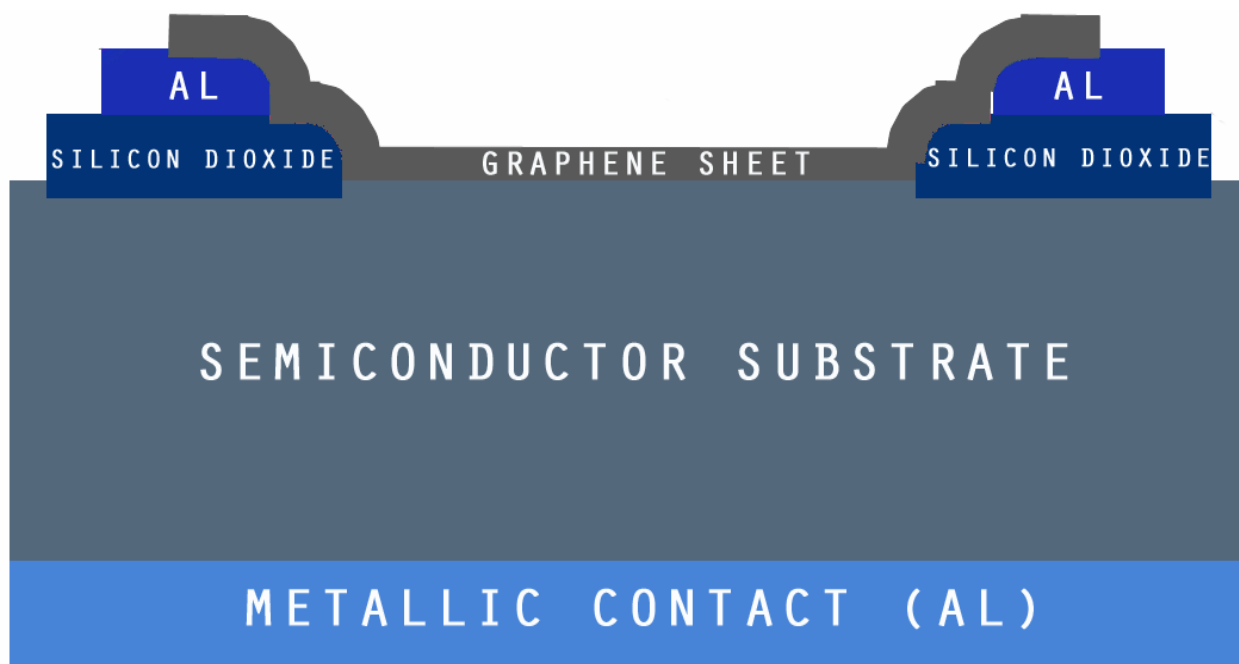


Figure 1. Proposed structure of Schottky graphene solar cell.

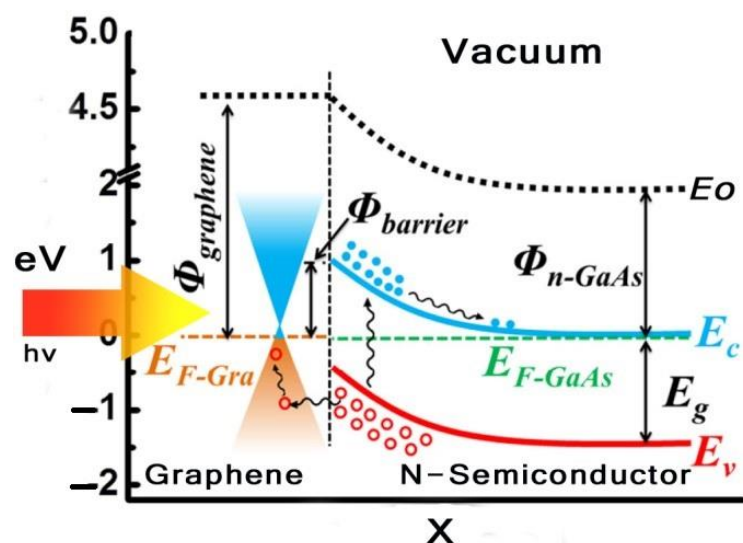


Figure 2. Energy band diagram of graphene solar cell.

The graphene GaAs and silicon junction solar cell are numerically simulated in this work using standard TCAD tools. It uses a typical method for materials such as amorphous, including state model of continuous density, auger recombination mechanisms, and Schottky, to solve continuity, Poisson, and current density equations. The dependence of these optical parameters with the photon energy has been included, taking into account the thickness of the substrate, work function of graphene, doping level, and their impact on cell efficiency.

2. Modelling Semi-Transparent Top-Layer Graphene in Atlas

Due to the fact that graphene is a novel material, it is not yet included in the SILVACO Atlas material library. As a result, in order to develop a reliable and exact model of the graphene film, the initial definition of the layer used 4H-SiC as the base material, which was then modified to give the metallic material properties and match experimental sheet resistance values [17]. First, the material 4H-SiC model was made entirely transparent without changing its optical characteristics. Next, the graphene transmittance was entered by creating an .nk file for graphene from the obtained value [18]. With $15,000 \text{ cm}^2/\text{Vs}$ of carrier mobility [19], graphene is described as the Fermi distribution, and band gap, effective masses, and thickness values of 10 nm were changed to make sure they matched the experimental findings. Table 1 is a list of the simulation parameters that the Atlas tool utilized for this cell [20].

Table 1. Material utilized in this numerical simulation.

Essential Layer Properties	ATLAS Identifier	Material Layer		
		Graphene	Substrate	
		4H-SiC	GaAs	Silicon
Band gap layer E_g (eV)	E_G	0.0	1.42	1.08
Relative permittivity, ϵ_r (F cm^{-1})	Permittivity	25	13.1	13.5
Electron affinity X_e (eV)	Affinity	5.8	4.07	4.17
Mobility, μ_p ($\text{cm}^2/\text{V s}$)	MUP	15,000	400	500
Mobility, μ_n ($\text{cm}^2/\text{V s}$)	MUN	15,000	8000	1000
Effective density of states N_c (cm^{-3})	NC300	3×10^{17}	4×10^{17}	2.8×10^{19}
Effective density of states N_v (cm^{-3})	NV300	3×10^{17}	7×10^{18}	1.0×10^{19}

3. Modelling Graphene-Based Solar Cells

With the use of TCAD, including the optical intensity, as shown in Figure 3, and using parameters from Table 1, the user of ATLAS can choose from a number of physics models to compute recombination and carrier mobility. We utilized the following models in our design for our analysis. The doping-dependent low-field mobilities of holes/electrons in the cell at 300 K were modelled. The recombination models utilized were the Optical Recombination (OPTR) and the Schottky–Read–Hall (SRH) recombination models. As already stated, Figure 4 shows the cross section of a graphene Si solar cell that was modelled in TCAD software. The device is made up of three areas, from bottom to top, namely the silicon substrate, the SiO_2 window, and the graphene layer. Here, an oxide window was used to coat the silicon substrate with a 10 nm thick layer of graphene. Figure 5 shows the detailed top layer of the cell.

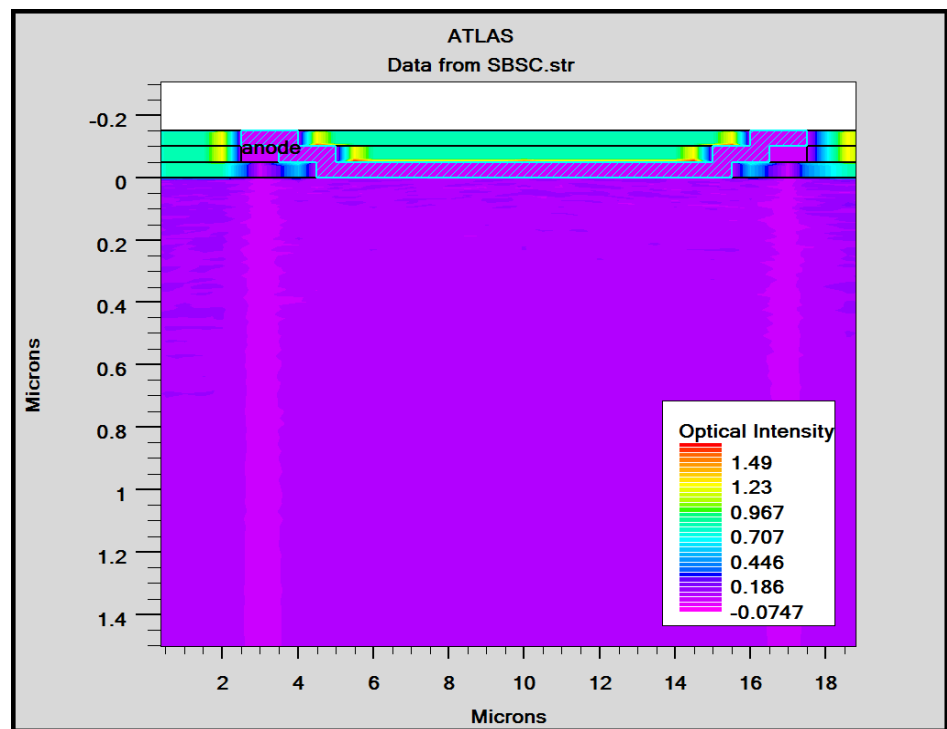


Figure 3. Optimized optical intensity in Si solar cell.

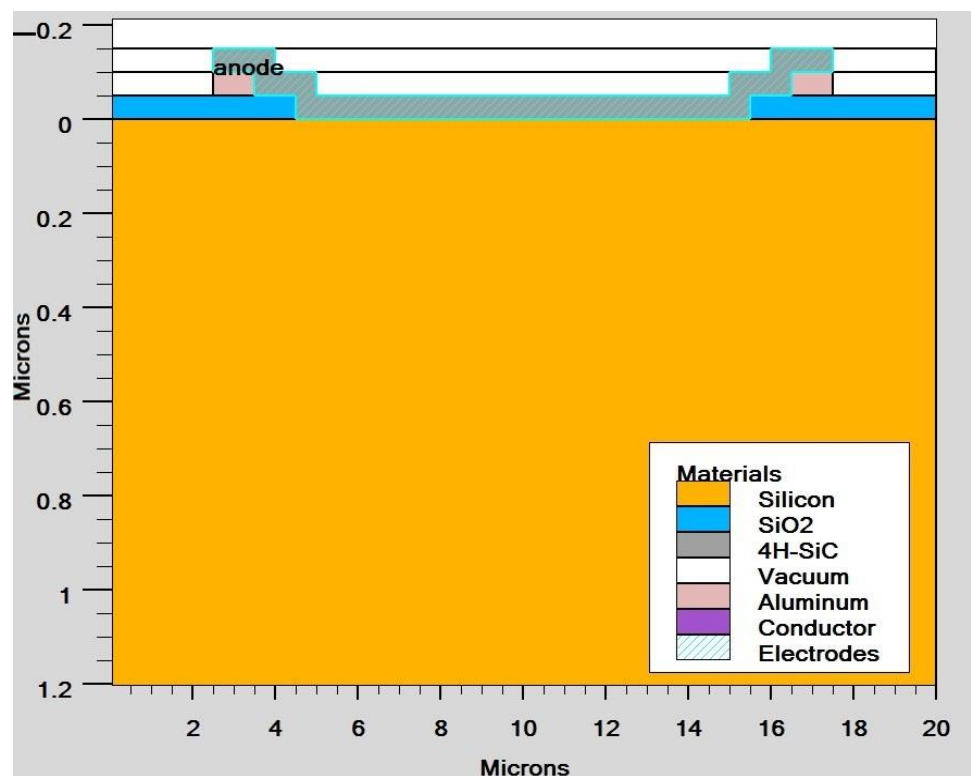


Figure 4. Solar cell cross-section view of graphene Si.

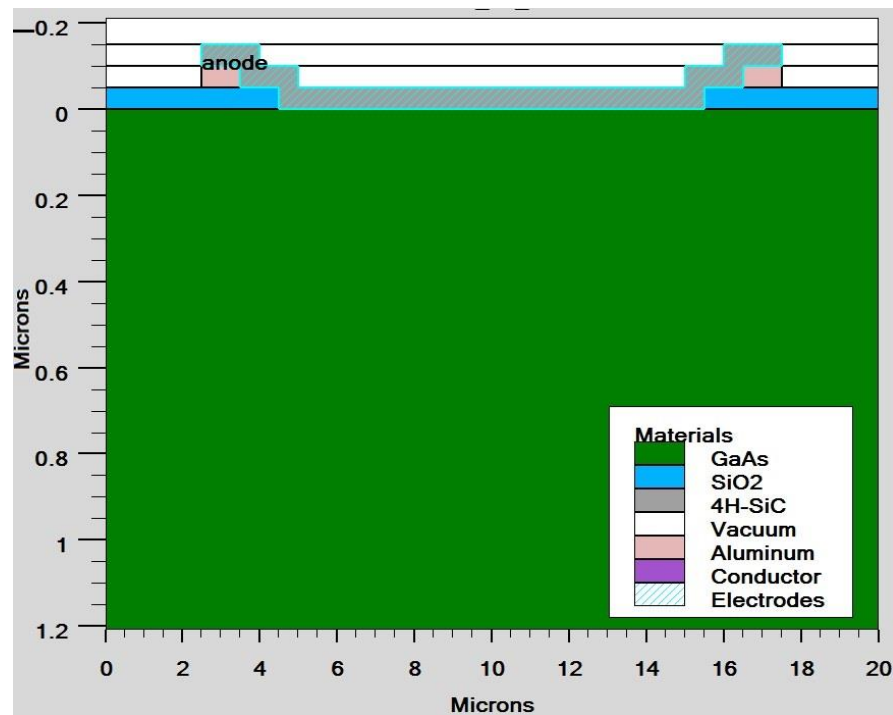


Figure 5. Solar cell cross-section view of graphene GaAs.

Most studies show that the heterojunction device for this structure is fabricated from a transferred chemical vapour deposition graphene layer on silicon in order to avoid expensive deposition methods and complicated processing [21,22]. In essence, the Schottky junction can be created using any semiconductor with a specific metal, provided the work function differences are sufficiently large and the carrier densities are moderate. The calculations show that graphene sheets and silicon create a Schottky junction, which is advantageous for creating a sizable built-in field [14]. The photoexcited holes and electrons are produced in the silicon substrate when it is illuminated, and they are subsequently separated at the Schottky junction through the built-in electric field. The bottom electrodes gather electrons/holes, leading to a photovoltaic reaction. The thermionic emission model can be used to describe the Schottky junction’s non-linear I-V property [23]:

$$I_o = \alpha B^* T^2 \exp(-e\phi_{Bn}/kT) \tag{1}$$

where α is area cell, B^* is effective Richardson constant, ϕ_{Bn} is metal–semiconductor (n-type), k is Boltzmann’s constant, and T absolute temperature.

$$\phi_B = \phi_G - \chi, \text{ for n-type semiconductor} \tag{2}$$

Additionally,

$$\phi_B = E_G - \phi_G + \chi, \text{ for p-type semiconductor} \tag{3}$$

where ϕ_G = graphene work function, χ = electron affinity, E_G = energy gap semiconductor.

4. Results and Discussion

In order to mimic the global terrestrial sunshine, the modelled device was illuminated with AM1.5G solar spectrum, which is taken into account by LUMINOUS 3D for modelling sunlight in SILVACO Atlas [24]. The light could be absorbed in the barrier layer and inside the semiconductor. The photogeneration rate is provided by $G = \eta_0 \frac{P\lambda}{hc} \alpha e^{-\alpha y}$, where P represents the total effect of the ray path’s absorption, reflection, and transmission losses, y

is the ray for the provided relative distance, α is the computed absorption coefficient for every combination value of (n, k) , λ is wavelength, h is Planck's constant, c is the speed of light, and η_0 is the internal quantum efficiency, denoting the carrier number produced per photon per pair. It can be seen from Figure 6 that the highest efficient absorption area is around 0.1 μm from the surface connection and it not only increases the light absorption length but is also concentrated to the light field, which results in enhanced excitation of photon-induced carriers. The recombination rate is also higher at the interface region, as indicated by the result shown in Figure 7. Figure 8 shows the potential developed inside the cell, indicating that maximum potential is developed in the anode vicinity and that there is a greater collection of charge. Figures 9–11 show a comparison of different thicknesses for the photogeneration rate, electric field, and potential, respectively. Figure 9a–c show the photogeneration rate of Si cells under AM1.5 (sun) with depths of absorption, which were examined at 5 μm , 10 μm , and 20 μm . The semiconductor and barrier could both absorb the light. Figure 9c shows that 20 μm thickness is more than sufficient for full-spectrum absorption because the intensity of the photogenerated carrier suddenly reduces in the deep area of the Si substrate. In Figure 10, as the number of solar cells rises, the electrical field also rises. In fact, an increase in the number of solar cells leads to an increase in the open-circuit photovoltage. The main aim of this paper is to enhance the conversion efficiency through a reduction in silicon matter. As a result, fewer solar cells must be utilised to generate the electrical field, which lowers the amount of semiconductor materials needed to make solar cells. Figure 10 gives the evolution of the electric field as a function of the solar cells. Figure 11 shows the potential developed inside the cell, showing that maximum potential is developed in the anode vicinity, indicating a greater collection of charge.

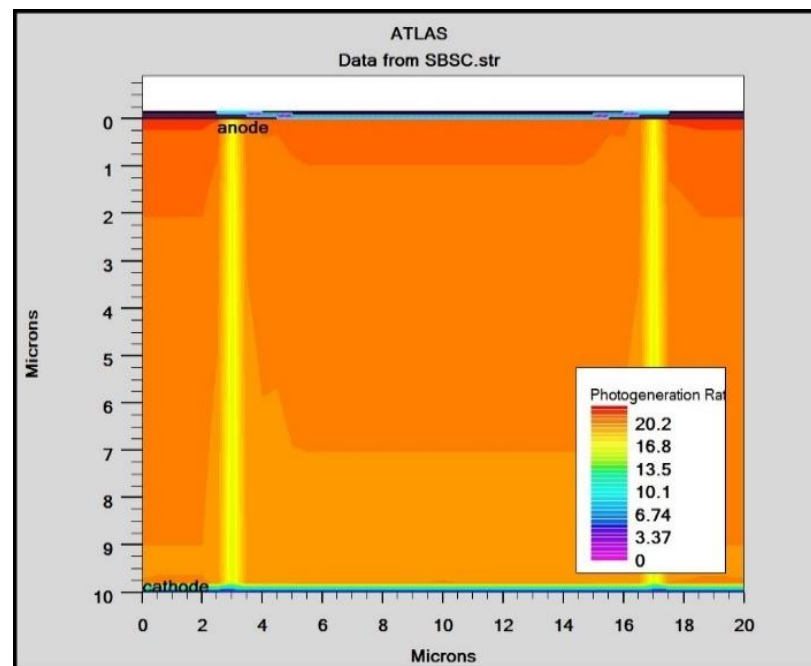


Figure 6. Photogeneration rate in Si solar cell.

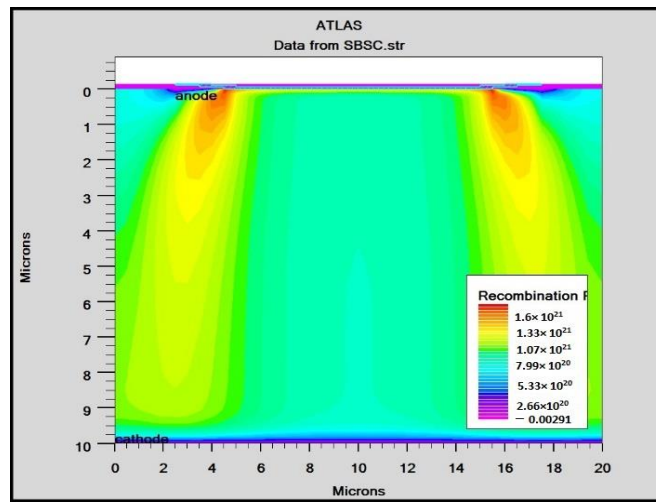


Figure 7. Recombination rate in Si Solar cell.

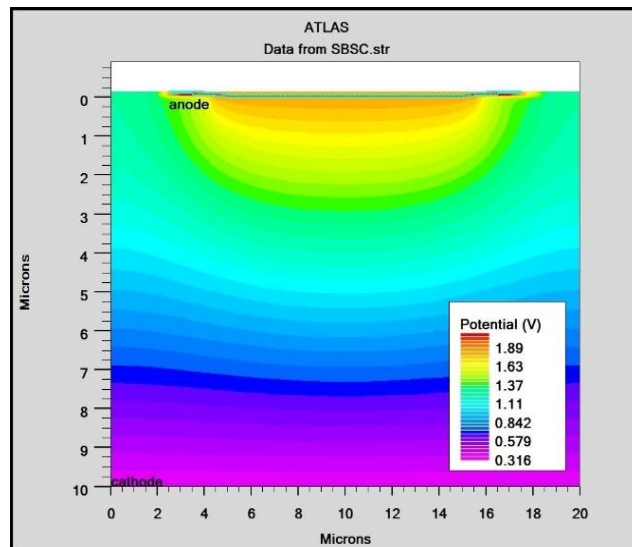


Figure 8. Potential of Si solar cell.

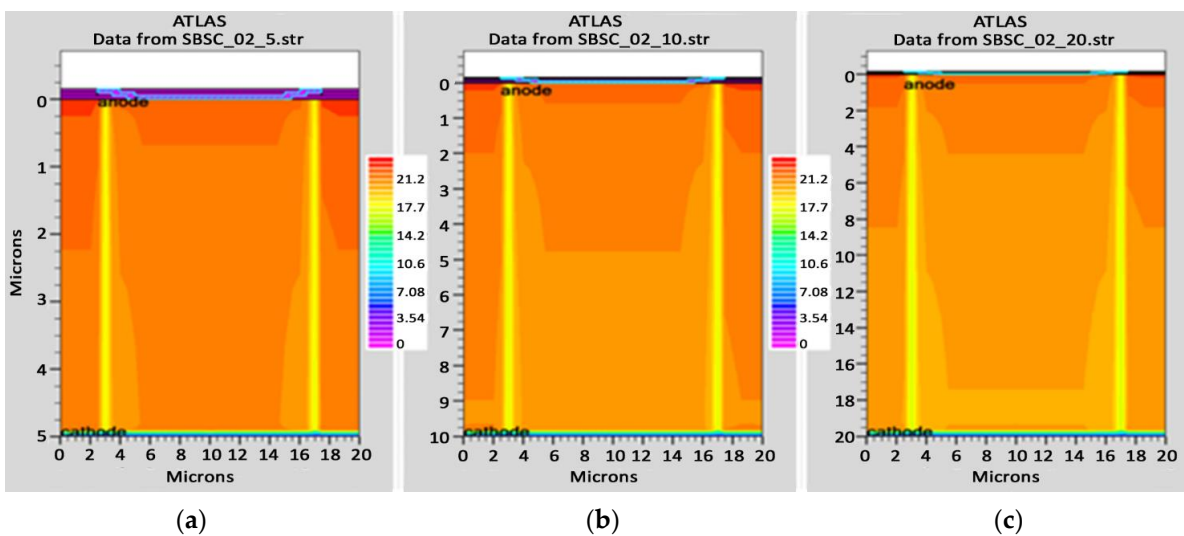


Figure 9. Photogeneration rate of Si cell: (a) 5 μm, (b) 10 μm, (c) 20 μm.

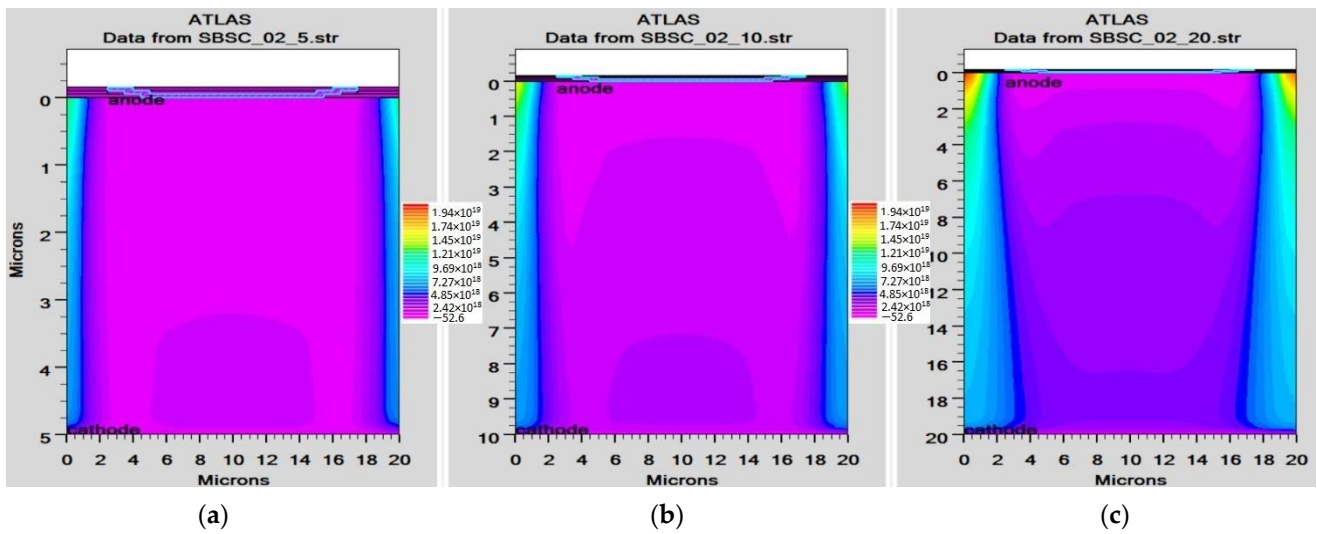


Figure 10. Electric field of Si cell: (a) 5 μm, (b) 10 μm, (c) 20 μm.

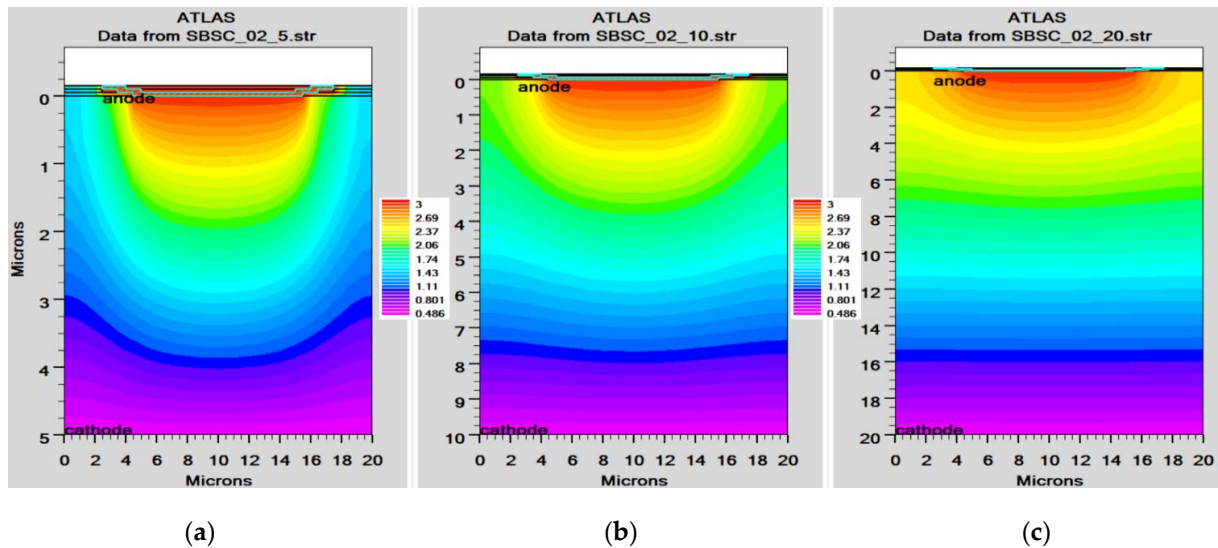


Figure 11. Potential of Si cell: (a) 5 μm, (b) 10 μm, (c) 20 μm.

It is crucial to utilize I_{SC} and V_{OC} to establish how well a solar cell works because they affect how much power it can produce.

$$V_{OC} = \frac{nKT}{q} \ln\left(\frac{I_L}{I_0} + 1\right) \tag{4}$$

$$FF = \frac{V_{OC} - \ln(V_{OC} + 0.72)}{V_{OC} + 1} = \frac{I_m V_m}{I_{SC} V_{OC}} \tag{5}$$

I_{SC} and V_{OC} utilisation at maximum power is measured via the fill factor. The efficiency can be expressed using FF as:

$$\eta = \frac{V_{OC} I_{SC} FF}{P_{in}} = \frac{P_{max}}{1000 [Wm^{-2}] \times CellArea [m^2]} \tag{6}$$

These are the performance metrics that we employed in our research for evaluating solar cells.

4.1. GaAs and Si Thickness Effect

The Si crystal substrate is illuminated with an orientation <100>. For photogenerated carrier intensity, graphene functions as a transparent electrode. The difference between the work functions was built using a Schottky junction. We computed the I-V curves and external quantum efficiency (EQE), as illustrated in Figures 12 and 13, respectively, to examine the impact of silicon thickness on solar cell performance. Since silicon has an indirect band gap, it works with longer wavelengths and results in higher quantum efficiency. When silicon crystal thickness decreases, long-wavelength light passes through the device and lowers the IQE. On the other hand, the enhanced recombination carrier rate on the back electrode causes a significant increase in the dark current. Because the silicon substrate is thicker, it is discovered that the efficiency of the device ranges from 2.37% to 5.99% (given in Table 2).

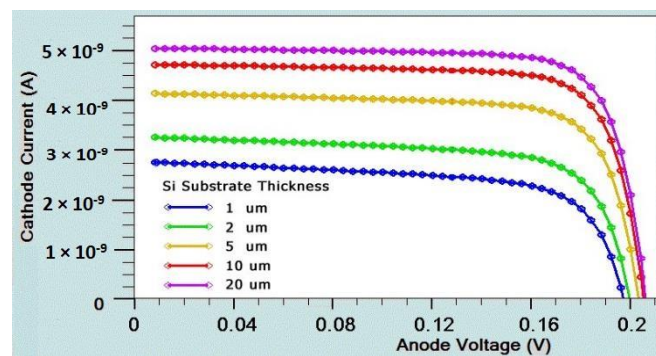


Figure 12. I-V curve of Si substrate with different thicknesses.

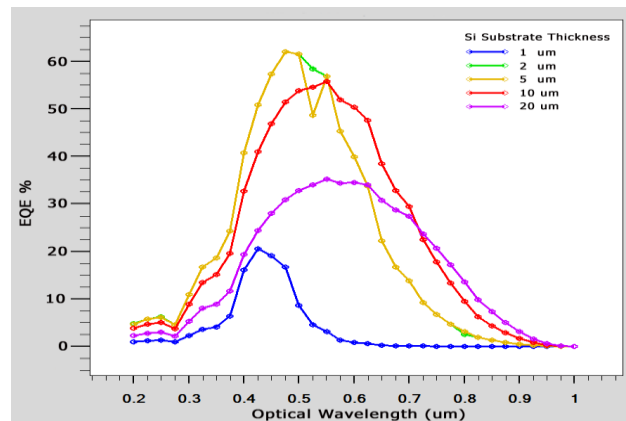


Figure 13. EQE of solar cell vs. different Si thicknesses.

Table 2. Performance of cell with substrate thickness (under n doping $3 \times 10^{16} \text{ cm}^{-3}$ and work function 4.8).

Thickness (μm)	J_{SC} (mA/cm^2)		V_{OC} (V)		FF (%)		Efficiency (%)	
	GaAs	Si	GaAs	Si	GaAs	Si	GaAs	Si
1	6.10	2.76	1.00	0.29	51	28.69	3.29	2.37
2	6.80	3.26	0.97	0.29	51	31.88	5.03	3.11
5	7.90	4.14	0.94	0.18	49	58.08	4.74	4.51
10	8.40	4.72	0.93	0.19	45	60.21	4.58	5.47
20	9.00	5.05	0.91	0.19	45	60.95	4.58	5.99

4.2. Graphene Work Function Effect

The difference between silicon χ and graphene ϕ_G is related to the barrier height ϕ_B , as discussed in Section 3. Therefore, a higher work function will enhance the ϕ_B , which will make the built-in potential V_{bi} increase according to the equation, $V_{bi} = \phi_B - V_n$, where V_n is the distance between E_c and E_f in silicon. Consequently, an enhanced graphene work function results in an increase in V_{bi} that corresponds to the upper limit of V_{oc} . As shown in Table 3, the built-in potential V_{bi} increases monotonically along with the FF and power conversion efficiency. This result is inconsistent with Y.F. Li's group's experimental findings [25].

Table 3. Performance of cell with graphene work function (under optimal 10 μm si-thickness).

Graphene Work Function	J_{SC} (mA/cm ²)		V_{OC} (V)		FF (%)		Efficiency (%)	
	GaAs	Si	GaAs	Si	GaAs	Si	GaAs	Si
4.4	6.10	4.72	1.00	0.18	51	50.34	3.29	4.9
4.6	6.10	4.72	0.97	0.16	51	48.21	5.03	5.3
4.8	6.10	4.72	0.94	0.19	49	60.21	4.74	5.4

4.3. GaAs and Silicon n-Type Doping Effect

The ability of silicon's N-type doping to raise the photogeneration carrier intensity and energy level of Fermi is well recognised. Due to the larger barrier height compared to a substrate made of pure silicon, both V_{OC} and I_{SC} increase for doping concentrations below $3 \times 10^{15} \text{ cm}^{-3}$. When the doping concentration exceeds $3 \times 10^{15} \text{ cm}^{-3}$, the cell's performance is radically different. The mechanism for electron emission could be the origin of this phenomenon. The emissions of a carrier from silicon to graphene are dominated by the tunnelling emission process rather than the thermionic emission mechanism. As a result, there is a slight decrease in the open-circuit voltage. Second, a high doping level reduces the photogeneration carriers' lifetime, particularly for light that has a long wavelength. These losses in the carrier collection result in a reduction in I_{SC} . Thirdly, as indicated in Table 4, the $3 \times 10^{16} \text{ cm}^{-3}$ doping level has the largest fill factor, despite having a lower power conversion efficiency than the other two doping concentrations. Therefore, the optimal efficiency is found at a moderate doping level of $3 \times 10^{15} \text{ cm}^{-3}$.

Table 4. Performance of cell with doping concentrations (under optimal 10 μm si- thickness).

Doping of n-Type Effect (/cm ⁻³)	J_{SC} (mA/cm ²)		V_{OC} (V)		FF (%)		Efficiency (%)	
	GaAs	Si	GaAs	Si	GaAs	Si	GaAs	Si
3×10^{14}	6.10	4.7	1.38	0.20	68	57.04	9.54	5.65
3×10^{15}	6.10	4.7	1.37	0.19	66	59.73	9.52	6.50
3×10^{16}	6.10	4.3	1.36	0.18	67	60.21	9.50	5.47

In order to improve the design, it is also necessary to identify different performance parameters. A solar cell I-V curve with varying substrate thicknesses is depicted in Figure 12. We determine the current–voltage curves and external quantum efficiency (EQE) for GaAs, as shown in Figures 14 and 15, respectively. It is found that Si EQE has well above 60% and GaAs EQE has 50%, which is optimized at the (2–5) μm substrate thickness due to the high photogeneration rate found at this substrate thickness.

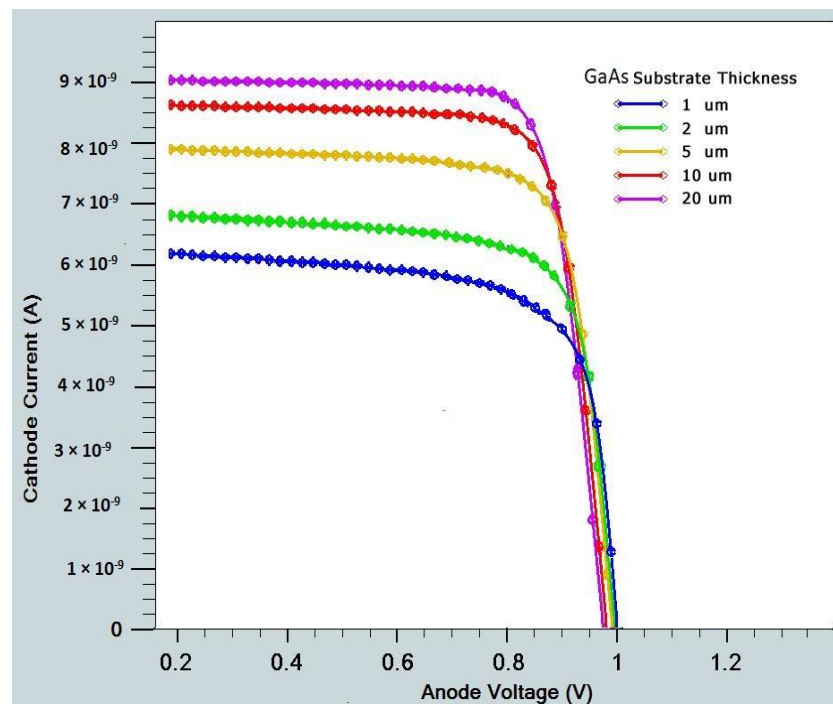


Figure 14. I-V curve of GaAs substrate with different thicknesses.

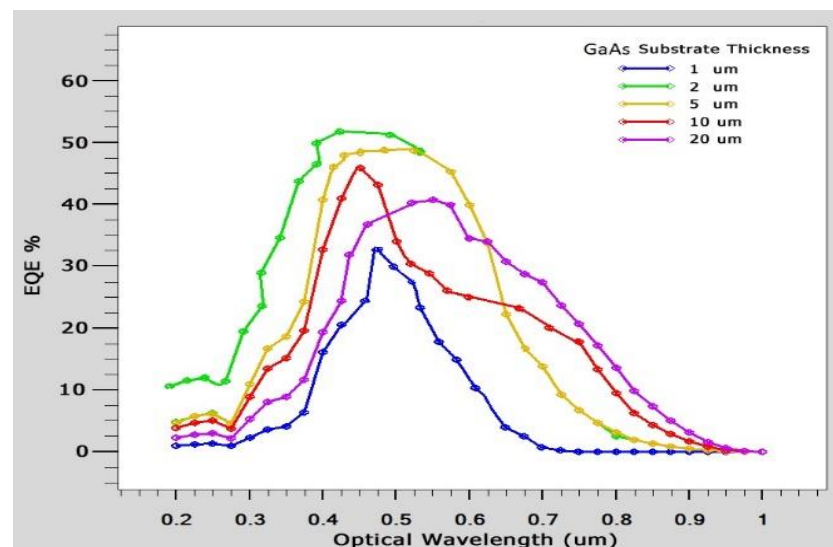


Figure 15. EQE of solar cell vs. different GaAs thicknesses.

The absorption and transmission co-efficient of the cell is depicted in Figure 16. The proposed cell works effectively in a wavelength range of 300 to 700 nm. After 700 nm, the efficiency starts decreasing due to an increase in transmittance and less absorptivity of photons, as shown in Figure 16. Most of the spectrum is found to be utilized in the generation of the carrier in the optimal 10 μm thickness Silicon substrate. Equation (7) can be used to determine J_{SC} using the measured EQE .

$$J_{SC} = q \int F(\lambda)EQE(\lambda)d\lambda \tag{7}$$

where $F(\lambda)$ = intensity spectrum of AM1.5G sunlight, and q is electron charge. It is found that EQE is well above 60%, which is an indication of an effective cell structure. Table 5 provides a tabular comparison that demonstrates that the Si substrate is significant when

compared with existing results. Through comparison with the existing results, it is found that graphene-based Schottky solar cells with Si and GaAs as substrates have increased efficiency of GaAs (4.74%) and Si (5.99%) over conventional Schottky junction solar cells.

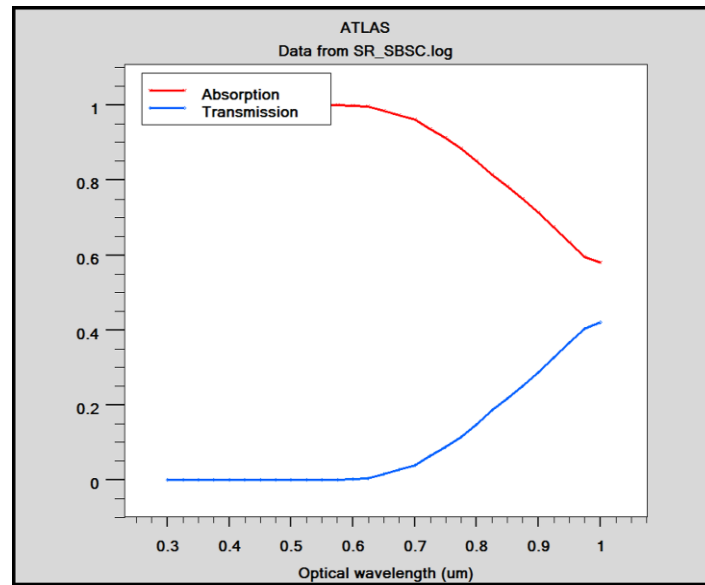


Figure 16. Absorption and transmission co-efficient of solar cells.

Table 5. Comparison of various factors, such as substrate thickness, work function, and doping concentration, with existing device.

	GaAs Thickness (μm)	Work Function (ev)	N-Type Doping (/cm ³)	<i>J</i> _{sc} (mA/cm ²)	<i>V</i> _{oc} (V)	<i>FF</i> (%)	Efficiency (%)
GaAs junction solar cell [26]	5	4.8	1 × 10 ¹⁴	7.966	0.301	49	1.518
Our proposed work	5	4.8	3 × 10 ¹⁶	6.10	0.94	49	4.74
	Si Thickness (μm)	Work Function (ev)	N-Type Doping (/cm ³)	<i>J</i> _{sc} (mA/cm ²)	<i>V</i> _{oc} (V)	<i>FF</i> (%)	Efficiency (%)
Si junction solar cell [27]	20	4..8	1 × 10 ¹⁷	5.72	0.158	58	0.874
Our proposed work	20	4..8	3 × 10 ¹⁶	5.05	0.19	60.95	5.99

5. Conclusions

Silvaco ATLAS software was used to model graphene-based GaAs solar cells and graphene-on-Si Schottky junction solar cells in a unique way for photovoltaic applications. Numerical simulation in two dimensions was used to analyze the output performance. Additionally, we thoroughly examined the performance vs. various graphene work functions, substrate thicknesses, and N-type doping concentrations. The findings demonstrate that greater graphene work function, adequate absorption thickness, and mild silicon doping are superior for increasing the power conversion efficiency. Further analysis revealed that the anode’s vicinity experienced the development of the highest potential, which leads to improved charge collection and an improvement in the solar cell’s overall performance. It is possible to research, design, and construct various structures of graphene-based solar cells using this remarkable optimization technique and data. The conversion of the emission electron mechanism from the thermionic mechanism to the tunnelling emission mechanism is due to the implementation of high-level doping, resulting in maximum *FF* but lower efficiency. For GaAs, under low illumination, the majority of the carriers created in the region reside relatively near to the interface. When compared to graphene’s lower transmittance and greater work function regarding cell performance, the work function is effective for increasing the cell performance. GaAs with moderate n-type doping has a significant increase in power con-

version efficiency; however, this form of device is significantly more sensitive to open-circuit voltage than short-circuit current. Therefore, Si has maximum conversion efficiency in terms of thicker absorption, larger graphene work function, and average doping in semiconductor substrates. As a result, it can be concluded from this work that graphene can function as a semi-transparent charge collector electrode and Schottky junction with a thermionic emission phenomenon for improved efficiency in SBSC solar cells.

Author Contributions: L.K.P., R.S.D. and K.J.S. conducted the experiment, design, material preparation, data analysis, and prepared most of the figures. R.S.D. Supervisor and K.J.S. Co-Supervisor of L.K.P. initiated the research and study and also contributed to the modeling and developing the novel idea and improvements in the manuscript. A.B. supported the work for the manuscript. All the authors discussed the results and contributed to the manuscript at various stages. R.S.D. and A.B. are the corresponding authors. The paper has two corresponding authors. All authors have read and agreed to the published version of the manuscript.

Funding: This work is partially supported by DST/TDT/DDP-38/2021, Device Development Programme (DDP), by the Department of Science & Technology (DST), Ministry of Science and Technology, Government of India.

Data Availability Statement: Not applicable.

Acknowledgments: The completion of this work would not have been possible without the support from Electronics and Communication Engineering Department, National Institute of Technology Mizoram, India.

Conflicts of Interest: The authors declare no conflict of interest.

References

1. Avouris, P.; Freitag, M. Graphene photonics, plasmonics, and optoelectronics. *IEEE J. Sel. Top. Quantum Electron.* **2014**, *20*, 6000112. [[CrossRef](#)]
2. Chen, D.; Zhang, H.; Liu, Y.; Li, J. Graphene and its derivatives for the development of solar cells, photoelectrochemical, and photocatalytic applications. *Energy Environ. Sci.* **2013**, *6*, 1362–1387. [[CrossRef](#)]
3. Gao, P.; Ding, K.; Wang, Y.; Ruan, K.; Diao, S.; Zhang, Q.; Sun, B.; Jie, J. Crystalline Si/graphene quantum dots heterojunction solar cells. *J. Phys. Chem. C* **2014**, *118*, 5164–5171. [[CrossRef](#)]
4. Zhang, Z.; Cui, T.; Lv, R.; Zhu, H.; Wang, K.; Wu, D.; Kang, F. Improved efficiency of Graphene/Si heterojunction solar cells by optimizing hydrocarbon feed rate. *J. Nanomater.* **2014**, *2014*, 359305. [[CrossRef](#)]
5. Miao, X.; Tongay, S.; Petterson, M.K.; Berke, K.; Rinzler, A.G.; Appleton, B.R.; Hebard, A.F. High Efficiency Graphene Solar Cells by Chemical Doping. *Nano Lett.* **2012**, *12*, 2745–2750. [[CrossRef](#)]
6. Lei, Y.; Li, R.; Chen, F.; Xu, J. Hydrothermal synthesis of graphene-CdS composites with improved photoelectric characteristics. *J. Mater. Sci. Mater. Electron.* **2014**, *25*, 3057–3061. [[CrossRef](#)]
7. Zhang, L.; Fan, L.; Wang, K. Graphene CdSe nanobelt solar cells with tunable configurations. *Nano Res.* **2011**, *9*, 891–900. [[CrossRef](#)]
8. Luo, L.B.; Chen, J.J.; Wang, M.Z.; Hu, H.; Wu, C.Y.; Li, Q.; Wang, L.; Huang, J.-A.; Liang, F.-X. Near-infrared light photovoltaic detector based on GaAs nanowire array/monolayer graphene Schottky junction. *Adv. Junctional Mater.* **2014**, *24*, 2794–2800. [[CrossRef](#)]
9. Jie, W.; Zheng, F.; Hao, J. Graphene/gallium arsenide-based Schottky junction solar cells. *Appl. Phys. Lett.* **2013**, *103*, 233111. [[CrossRef](#)]
10. Aukerman, L.W.; Dvis, P.W.; Graft, R.D.; Shilliday, T.S. Radiation effects in GaAs. *J. Appl. Phys.* **1963**, *34*, 3590–3599. [[CrossRef](#)]
11. Dohler, G.H.; Kunzel, H.; Olego, D.; Ploog, K.; Ruden, P.; Stolz, H.J.; Abstreiter, G. Observation of tunable band gap and two-dimensional subbands in a novel GaAs superlattice. *Phys. Rev. Lett.* **1981**, *47*, 864. [[CrossRef](#)]
12. Tingting, F. Graphene based schottky junction solar cells on patterned silicon pillar array substrate. *Appl. Phys. Lett.* **2011**, *99*, 23505.
13. Behura, S.K.; Nayak, S.; Mukhopadhyay, I.; Jani, O. Junction characteristics of chemically-derived graphene/p-Si heterojunction solar cell. *Carbon* **2014**, *67*, 766–774. [[CrossRef](#)]
14. Li, X. Graphene on silicon schottky junction solar cells. *Adv. Mater.* **2010**, *22*, 2743–2748. [[CrossRef](#)] [[PubMed](#)]
15. Xie, C.; Jie, J.; Nie, B.; Yan, T.; Li, Q.; Lv, P.; Li, F.; Wang, M.; Wu, C.; Wang, L.; et al. Schottky solar cells based on graphene nanoribbon/multiple silicon nanowires junctions. *Appl. Phys. Lett.* **2012**, *100*, 193103. [[CrossRef](#)]
16. Zhang, X. High efficiency graphene/Si nanoarray schottky junction solar cells via surface modification and graphene doping. *J. Mater. Chem. A* **2013**, *1*, 6593–6601. [[CrossRef](#)]
17. Nair, R.R.; Blake, P.; Grigorenko, A.N.; Novoselov, K.S.; Booth, T.J.; Stauber, T.; Peres, N.M.R.; Geim, A.K. Fine Structure Constant Defines Visual Transparency of Graphene. *Science* **2008**, *320*, 1308. [[CrossRef](#)]

18. Weber, J.W.; Calado, V.E.; Van De Sanden, M.C.M. Optical constants of graphene measured by spectroscopic ellipsometry. *Appl. Phys. Lett.* **2010**, *97*, 091904. [[CrossRef](#)]
19. Arefinia, Z.; Asgari, A. A new modeling approach for graphene based silicon nanowire Schottky junction solar cells. *J. Renew. Sustain. Energy* **2014**, *6*, 043132. [[CrossRef](#)]
20. Silvaco. *Atlas User's Manual*; Silvaco: Santa Clara, CA, USA, 2014; pp. 163–165.
21. Lancellotti, L.; Polichetti, T.; Ricciardella, F.; Tari, O.; Gnanapragasam, S.; Daliento, S.; Di Francia, G. Graphene applications in Schottky barrier solar cells. *Thin Solid Film.* **2012**, *522*, 390–394. [[CrossRef](#)]
22. Cui, T. Enhanced efficiency of graphene/silicon heterojunction solar cells by molecular doping. *J. Mater. Chem. A* **2013**, *1*, 5736–5740. [[CrossRef](#)]
23. Sze, S.M.; Li, Y.; Ng, K.K. *Physics of Semiconductor Devices*; John Wiley & Sons: Hoboken, NJ, USA, 1981.
24. Singh, K.J.; Chettri, D.; Singh, T.J.; Thingujam, T.; Sarkar, S.K. A performance optimization and analysis of graphene based Schottky barrier GaAs solar cell. In Proceedings of the International Conference on Aerospace, Mechanical and Mechatronic Engineering, Bangkok, Thailand, 21–23 April 2017; IOP Publishing: Bristol, UK, 2017; Volume 211, p. 012024.
25. Li, Y.F.; Yang, W.; Tu, Z.Q.; Liu, Z.C.; Yang, F.; Zhang, L.Q.; Hatakeyama, R. Schottky junction solar cells based on graphene with different numbers of layers. *Appl. Phys. Lett.* **2014**, *104*, 043903. [[CrossRef](#)]
26. Kaung, Y. Modeling and design of graphene GaAs junction solar cell. *Hindawi. Adv. Condens. Matter Phys.* **2015**, *2015*, 326384. [[CrossRef](#)]
27. Kaung, Y.; Lui, Y.; Ma, Y.; Xu, J.; Yang, X.; Feng, J. TCAD analysis of graphene silicon Schottky junction solar cell. In Proceedings of the International Symposium on Photonics and Optoelectronics, Shanghai, China, 22–24 August 2015; Volume s9656.

Disclaimer/Publisher's Note: The statements, opinions and data contained in all publications are solely those of the individual author(s) and contributor(s) and not of MDPI and/or the editor(s). MDPI and/or the editor(s) disclaim responsibility for any injury to people or property resulting from any ideas, methods, instructions or products referred to in the content.